THE JOURNAL OF PHYSICAL CHEMISTRY C

ARTICLE

pubs.acs.org/JPCC

Graphene Formation by Decomposition of C_{60}

Luís M.A. Perdigão,* Syarifah N. Sabki, Jason M. Garfitt, Pierre Capiod, and Peter H. Beton

School of Physics and Astronomy, University of Nottingham, University Park, Nottingham NG7 2RD, U.K.

ABSTRACT: Graphene is formed through the thermally induced decomposition of C_{60} in combination with a Ni thin film. After transfer to a SiO_2 substrate, optical microscopy and Raman spectroscopy confirm the presence of graphene for films of C_{60} buried under nickel or alternatively for C_{60} adsorbed on a nickel surface. For buried films the graphene thickness is shown to depend on the fullerene dosage, with evidence of domain growth from nucleation sites separated by tens of micrometers. The adsorption of C_{60} and the changes arising from annealing are also monitored using scanning tunneling microscopy. We relate our results to previous studies of the decomposition of C_{60} on nickel and other transition metals.

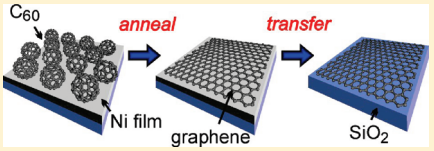

INTRODUCTION

Monolayer graphene consists of a single atomic layer of sp^2 hybridized carbon atoms which are bonded in a honeycomb array and has been grown and widely investigated on metallic substrates[1−3] under ultrahigh vacuum conditions in a series of studies dating back over many years. Following the demonstration by Novoselov et al.[4] that single sheets of graphene could be isolated and transferred to other substrates using an exfoliation method and the growth of graphene on SiC,[5] there has been renewed interest in the growth of graphene to provide large areas of material[6−21] for a variety of applications. The great interest in the controlled production of graphene arises from its exceptional electronic properties, and this material has great technological potential for the fabrication of new electronic devices and sensors.[22]

In recent reports, the formation of graphene on metal surfaces such as nickel or copper is commonly achieved by chemical vapor deposition (CVD) using a gaseous hydrocarbon source such as methane, ethene, or propene[6,14−17] and differs from early studies in that the growth does not occur under ultrahigh vacuum conditions but under much higher pressures, even up to ambient pressure. Recently, Yu et al.[14] and others[6,15−18] have shown that graphene grown by this route can be released from the metal substrate by chemical etching. The resulting graphene has overall thicknesses down to the few-layer or monolayer and can be transferred to other surfaces.

It is also possible to form graphene from sources other than gaseous hydrocarbons. In recent work, we have demonstrated that immersion of a Rh film in an organic solvent followed by a thermal anneal in vacuum can lead to the formation of graphene.[23,24] It has also been shown that annealing nickel films on SiO_2 surfaces can lead to the formation of graphene, due to trace background carbon contamination[25] or the intentional inclusion of amorphous carbon.[26] The solid-state reaction relevant to these latter processes has been studied previously by Shelton et al.,[27] Eizenberg et al.,[28] and Fujita et al.[29,30] using carbon-doped polycrystalline nickel, and an alternative approach to the formation of graphene from solid sources on copper films has also been recently reported.[31]

In this paper, we investigate the use of a molecular source of carbon for the formation of graphene in conjunction with a nickel thin film. Specifically we demonstrate the formation of graphene on nickel films using C_{60} as a carbon source. C_{60} is chosen since the overall dosage of sublimed molecular layers can be controlled down to the submonolayer level, and it is also known that C_{60} decomposes on a nickel surface,[32,33] although the resulting product of this decomposition has not hitherto been identified. Graphene films prepared from C_{60} were transferred to a SiO_2 surface, and their quality was analyzed using Raman spectroscopy. The conversion of C_{60} to graphene was also studied in situ using scanning tunneling microscopy (STM).

EXPERIMENTAL METHODS

Our experiments are typically performed using nickel thin films deposited on SiO_2 (thickness 300 nm) grown thermally on a Si(100) wafer apart from a small number of samples which were grown on sapphire for use in STM investigations. Initially 7 × 10 mm^2 pieces of Si/SiO_2 are loaded in a vacuum system (base pressure 10^{-8} Torr) and degassed at 800 °C in 10^{-8} mbar vacuum conditions for over one hour (omission of this step leads to the formation of graphene even for control samples with no intentionally added carbon as previously reported;[25] this indicates that carbon-containing adsorbed species present on the SiO_2 surface prior to nickel deposition can be transformed into a surface graphene layer if this preparative procedure is omitted).

Sample heating was achieved by passing a current through a piece of highly doped silicon placed at the back of the SiO_2 sample wafer, and the surface temperature was measured using a pyrometer. Nickel was evaporated using an integral tungsten−alumina crucible, and the film thickness (typically 100 nm) was measured using a quartz microbalance. C_{60} was sublimed from a Knudsen cell at constant temperature with a deposition rate of 0.16 nm/min (0.8 nm of C_{60} is equivalent to 1 monolayer, which has a surface density of 1.2 × 10^6 molecules/μm^2). The samples were then annealed at 650−890 °C for 2−15 min. Following annealing the current on the silicon back heater was reduced to zero over a controlled period, typically 15 s.

Transfer of the graphene films was then performed using a variation of the technique described previously,[14−16,25] in which

Received: December 2, 2010
Revised: March 9, 2011
Published: March 25, 2011

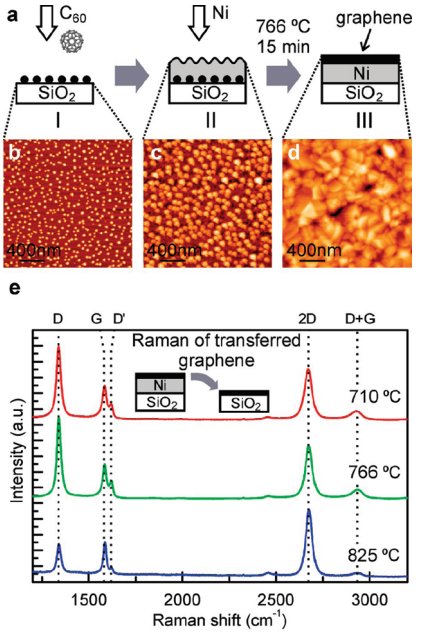

Figure 1. Graphene synthesized from C_{60} buried under a nickel film on a SiO_2 surface. **a** Shows the preparation procedure done in vacuum: (I) ~1.6 nm of C_{60} was deposited on a predegassed SiO_2 surface, (II) nickel film was grown by evaporation, and then (III) the whole assembly was annealed at a chosen temperature for 15 min. **b**, **c**, and **d** are tapping mode 2 × 2 μm AFM images of the samples taken out after each of the stages I, II, and III, respectively. **e** is the Raman spectra of transferred graphene prepared at different annealing temperatures given, with the peaks D, G, D′, 2D, and D + G assignment shown with dashed lines.

$FeCl_3$ is used to etch the nickel leaving the graphene attached to supporting polymer layers (PMMA/PDMS was used in this study). The graphene/polymer layer was placed on a separate substrate (90 nm SiO_2 oxide grown thermally on Si) and immersed in acetone to dissolve the PMMA and release the graphene. The resulting layer is optically visible[34] and was characterized using Raman spectroscopy (Horiba Scientific LabRAM HR) with an excitation wavelength of 532 nm. STM images are acquired in a vacuum using a commercial (Nanograph Systems) instrument which is operated at room temperature using Pt/Ir cut tips. Ambient STM images were acquired using a commercial instrument (Molecular Imaging/Agilent) also using cut Pt/Ir tips.

RESULTS AND DISCUSSION

Two methods were used to grow the graphene films, which differ in the order that the C_{60} and nickel were deposited. We consider first the deposition of nickel on C_{60}. Initially, 1.6 nm of C_{60} was deposited on the SiO_2 surface leading to the formation of islands with typical width separations of 40 and 100 nm, respectively (see images acquired using atomic force microscopy, AFM, in Figure 1; average island height 14 nm), consistent with a Volmer−Weber growth mode. After overgrowth of nickel, protrusions of similar dimensions are observed in the surface topography suggesting that the C_{60} islands are not significantly disrupted by the deposition of nickel. After the Ni/C_{60} layers are annealed, the island topography is no longer observed. Instead we observe a polycrystalline faceted morphology which is essentially identical to that observed for an annealed nickel film in the absence of C_{60}. This change in topography indicates a significant reordering of surface constituents. In the second procedure (see Figure 2a), the order of deposition is

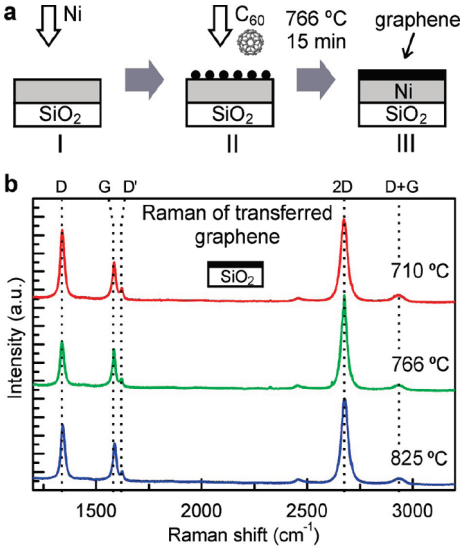

Figure 2. Graphene synthesized from 1.6 nm of C_{60} deposited over a nickel film on a SiO_2 surface. **a** shows the procedure used: (I) nickel film was grown on predegassed SiO_2 piece, (II) sample was exposed to C_{60}, and (III) then the sample was annealed for 15 min. **b** is the Raman spectra of post-transferred graphene versus annealing temperature.

reversed so that nickel is first deposited on the SiO_2 surface followed by deposition of C_{60} and then annealed.

After the etch-release of the surface layers, the presence of graphene was confirmed using Raman spectroscopy. The spectra in Figures 1e and 2b were acquired for, respectively, buried C_{60} and C_{60}-on-nickel, that were annealed at 710, 766, and 825 °C for 15 min. Annealing at 880 °C resulted in no transferred graphene. Several peaks associated with the presence of graphene are easily identified in all spectra, the D (1356 cm^{-1}), G (1581 cm^{-1}), D′ (1620 cm^{-1}), 2D (2688−2728 cm^{-1}), and D + G (2950 cm^{-1}) peaks.[35] The spectral intensity was normalized to the intensity of the G peak, and selected peak intensities for each temperature are presented in Table 1.

The 2D peak (2688−2728 cm^{-1}) arises from the second-order breathing mode of a single phenyl ring on the graphene,[35] and the intensity and position of this peak are sensitive to the number of graphene layers. For monolayer graphene, a single Lorentzian with full-width-half-maximum (fwhm) ~30 cm^{-1} and normalized intensity (I_{2D}/I_G) ranging from ~1 to 2 (<1 for multilayers) are expected.[35] On the graphene obtained from buried C_{60} there is an increase of the I_{2D}/I_G ratio for higher annealing temperatures. For graphene grown with C_{60} on nickel, the I_{2D}/I_G is generally higher, suggesting a higher monolayer fraction, while for these samples the fwhm is lower and has less variation with annealing temperature. These results suggest that single graphene layers are best achieved with C_{60} deposited on top of the nickel film and at annealing temperatures of 760−825 °C. Higher-temperature annealing results in a lower number of graphene layers consistent with studies by Shelton et al.,[27] Fujita et al.,[29] and Eizenberg et al.[28] on carbon-doped nickel. The Raman spectra in Figures 1e and 2b have an I_D/I_G intensity which indicates a significant level of disorder. We investigated the effect of the postannealing cooling rate, which is known to limit carbon segregation and solvation during the cooling process in graphene grown by CVD.[14] An increase in cooling rate leads to a small reduction of the D peak to values $I_D/I_G < 1$.

Table 1. Summary of Measured Values Obtained from the Raman Spectra of Transferred Graphene, Prepared with C_{60} under and above the Nickel Film and Annealed at Different Temperatures[a]

	anneal temperature	D peak	2D peak		
	°C	I_D/I_G	I_{2D}/I_G	position/cm^{-1}	fwhm/cm^{-1}
nickel on C_{60}	710	2.31	1.61	2674.3	41.3
	766	2.64	1.68	2675.7	37.7
	825	0.95	2.18	2677.1	35.6
C_{60} on nickel	710	1.94	2.33	2670.0	34.9
	766	1.26	2.40	2674.3	31.0
	825	1.53	2.39	2674.3	33.5

[a] The D peak and 2D peak intensities are normalized to the intensity of the G peak. The position and fwhm of the 2D peak are also given

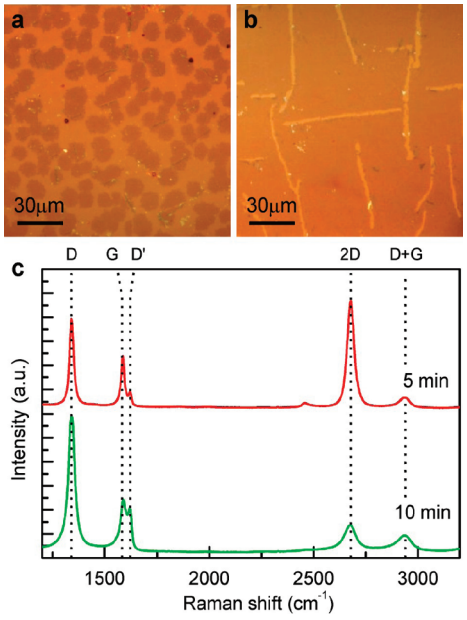

Figure 3. **a** and **b** are 150 × 150 μm optical microscope images of transferred graphene produced using the buried C_{60} method with exposure to 0.8 nm (5 min) and 1.6 nm (10 min) of C_{60}, respectively. Darker and lighter contrasts are graphene and bare SiO_2, respectively. **c** is the Raman spectra of the graphene regions in images **a** (green) and **b** (red).

The effect of varying C_{60} dosage was also studied (see the optical micrographs in Figures 3a and 3b). For low coverage (0.8 nm of buried C_{60}, see Figure 3a) we observe the formation of isolated near-circular islands of graphene (darker regions) with typical diameters and separations of 10 μm. A Raman spectrum acquired for such an island is shown in Figure 3c (red line) and, with a ratio of $I_{2D}/I_G \sim 2$, is consistent with monolayer graphene. Higher coverage of C_{60} (1.6 nm of buried C_{60}) results in near complete sample coverage (Figure 3b) and multiple layers as deduced from the 2D peak in the Raman spectra (Figure 3c, green line) which has a fwhm ~47 nm and $I_{2D}/I_G < 1$. This result shows clearly that the graphene layer thickness can be controlled by varying the coverage of C_{60}. In addition, our results show that, following nucleation, graphene initially grows as a monolayer. The use of a buried C_{60} layer is somewhat analogous to the use of amorphous carbon[26] although there are several differences in the Raman spectra we observe for a fullerene source of carbon. In particular, the 2D peak is much narrower in the current work indicating a high fraction (50%) of monolayer graphene.

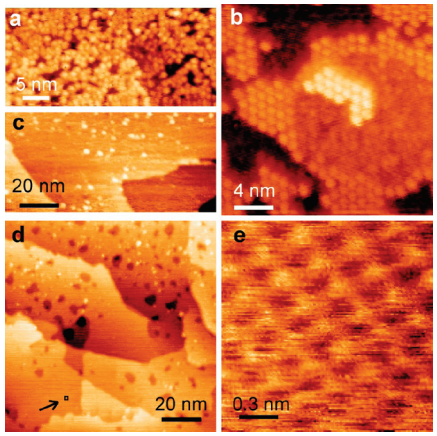

Figure 4. Succession of STM images acquired during preparation of the C_{60}−Ni−sapphire sample. **a** STM image obtained after ~1 monolayer C_{60} deposited onto 100 nm of nickel film on sapphire. Image **b** was obtained after annealing the C_{60}−Ni−sapphire to 540 °C for 10 min, demonstrating that the C_{60} reordered and formed well-ordered islands. **c** shows the STM image obtained after additional annealing to 595 °C for 10 min. **d** was obtained with an ambient-STM after taking the sample from the vacuum chamber to air. Image **e** was scanned in the square region indicated with an arrow in **d**. Tunneling parameters are: **a** −0.5 V, 0.1 nA; **b** +0.3 V, 0.3 nA; **c** −1.0 V, 0.1 nA; **d** −0.3 V, 1.0 nA; **e** −0.2 V, 1.0 nA.

It is possible to estimate the fraction of deposited carbon atoms that is incorporated in the graphene. A C_{60} layer with average thickness 0.8 nm (1 monolayer) has a carbon content equivalent to ~3.2 monolayers of graphene, but as shown in Figure 3 an annealed film with this coverage actually results in a lower overall coverage of ~0.5 monolayers. We believe that the remaining carbon forms pyrolitic carbon (PyC) at the nickel−SiO_2 interface or remains dissolved within the nickel. Evidence for the formation of PyC is provided by Raman spectroscopy and optical imaging of the SiO_2/Ni interfacial region following etching (in this case no transfer was performed, and the resulting carbon layers remained on the substrate used for growth), which confirmed the presence of a material with very wide D and G bands similar to the spectra for PyC formed by CVD on SiO_2.[36]

Further insight into the transformation of C_{60} to graphene can be obtained by monitoring the nickel surface using STM. For these experiments, we use sapphire as a substrate since the resulting nickel films are flatter (following annealing at 710 °C for ~10 min) and therefore more compatible with STM imaging. Figure 4a shows an image acquired following deposition of 1 monolayer of C_{60}.

Although the overall arrangement is disordered, it is possible to resolve individual molecules. After annealing the sample at 540 °C for 10 min (Figure 4b) well-ordered hexagonal close-packed islands are observed with an apparent height of 0.42 nm. Kusch et al. have previously investigated the adsorption of C_{60} on Ni(111) using low-energy electron diffraction (LEED).[32] These authors find that, similar to our STM results, adsorption at room temperature leads to a disordered arrangement, but a hexagonally ordered phase is formed following annealing. The temperature we observe for the transition from disordered to well-ordered C_{60} domains is in good agreement with the value of 530 °C reported by Kusch et al.[31] The measured intermolecular C_{60} distance of 1.0 nm matches well with a 4×4 periodicity with the Ni(111) surface ($a_{Ni} = 0.249$ nm, $4 \times a_{Ni} = 0.996$ nm). The estimated fractional C_{60} coverage is reduced to ~0.5 ML at this stage. Annealing at higher temperature, 595 °C, results in a change of the surface morphology (Figure 4c), with an absence of C_{60} domains of molecules, but the nickel terrace structure remains essentially unchanged. Our results indicate that dissociation of C_{60} occurs between 540 and 595 °C since we have found that graphene is present for samples annealed at >600 °C. This result is fully consistent with previous studies of C_{60} on Ni(111), while on Ni(110) decomposition and conversion to a graphitic layer have also been reported, but at a slightly lower temperature (490 °C).[33] Additional annealing at 655 and 710 °C did not cause a significant change of morphology.

Images of the surface have also been acquired using an ambient-STM following transfer of the sample to atmosphere. Figures 4d and 4e show an overall morphology that is very similar to that observed in vacuum apart from the presence of shallow holes (Figure 4d). A zoomed image in the region indicated with an arrow is shown in Figure 4e and shows a regular structure with a period $\sim 0.24 \pm 0.01$ nm, close to the expected surface lattice constant of graphite/graphene and similar to previously published images of graphene on nickel.[17,37] The presence of graphene is confirmed by applying the polymer-etching-transfer procedure to this sample. The resulting Raman spectra confirm the presence of ~2 layers of graphene. As noted in a previous publication, the graphene layer inhibits oxidation of the metal surface,[25] and we believe this facilitates the ambient STM studies. We attribute the presence of pits, which are typically up to 1.5 nm deep, to defects in the graphene layer which allow, and possibly arise from, localized oxidation of the graphene/nickel surface.

CONCLUSIONS

To conclude, we have shown that the decomposition of C_{60} on nickel, which has previously been reported in the literature, provides graphene as a product. The formation of graphene has been verified by releasing the resulting layers by etching the metal substrate. The C_{60} coverage, annealing temperature, and deposition sequence were all found to influence the properties of the graphene layers, and this molecular source of carbon provides a method of controlling the total dosage of carbon introduced into the film with a high degree of precision. Raman spectra acquired for our transferred films indicate that the films grown using fullerene have a high monolayer fraction but also a higher defect (D) peak than is commonly observed for CVD few-layer graphene grown on nickel. It is possible that the film quality can be further improved using other metals or different molecular precursors while retaining the high monolayer fraction we observe. In conjunction with our previous report of graphene growth,[25] it is also clear that carbon present at a buried metal/SiO_2 layer can diffuse and segregate at the surface, and graphene growth can even arise from adsorbed carbon unless this is removed by annealing, or some other process, prior to metal deposition. Overall, our results provide an alternative solid-state approach for the formation of graphene with controlled layer thickness.

AUTHOR INFORMATION

Corresponding Author
*E-mail: luis.perdigao@nottingham.ac.uk.

ACKNOWLEDGMENT

This work was funded by the UK Engineering and Physical Sciences Research Council under grant EP/D048761/1. We acknowledge the Nottingham Nanotechnology and Nanoscience Centre for giving access to the Raman system and the East Midlands Development Agency for funding this equipment. S.N.S. is grateful for funding provided by the Ministry of Higher Education Malaysia and from Universiti Malaysia Perlis (UniMAP).

REFERENCES

(1) Rosei, R.; De Crescenzi, M.; Sette, F.; Quaresima, C.; Savoia, A.; Perfetti, P. *Phys. Rev. B* **1983**, *28*, 1161.
(2) Nagashima, A.; Tejima, N.; Oshima, C. *Phys. Rev. B* **1994**, *50*, 17487.
(3) Land, T. A.; Michely, T.; Behm, R. J.; Hemminger, J. C.; Comsa, G. *Surf. Sci.* **1992**, *264*, 261.
(4) Novoselov, K. S.; Geim, A. K.; Morozov, S. V.; Jiang, D.; Zhang, Y.; Dubonos, S. V.; Grigorieva, I. V.; Firsov, A. A. *Science* **2004**, *306*, 666–669.
(5) Berger, C.; Song, Z.; Li, T.; Li, X.; Ogbazghi, A. Y.; Feng, R.; Dai, Z.; Marchenkov, A. N.; Conrad, E. H.; First, P. N.; de Heer, W. A. *J. Phys. Chem. B* **2004**, *108*, 19912–19916.
(6) Li, X.; Cai, W.; An, J.; Kim, S.; Nah, J.; Yang, D.; Piner, R.; Velamakanni, A.; Jung, I.; Tutuc, E.; Banerjee, S. K.; Colombo, L.; Ruoff, R. S. *Science* **2009**, *324*, 1312–1314.
(7) Obraztsov, A.; Obraztsova, E.; Tyurnina, A.; Zolotukhin, A. *Carbon* **2007**, *45*, 2017–2021.
(8) Sutter, P. W.; Flege, J.; Sutter, E. A. *Nat. Mater.* **2008**, *7* 406–411.
(9) Martoccia, D.; Willmott, P. R.; Brugger, T.; Björck, M.; Günther, S.; Schlepütz, C. M.; Cervellino, A.; Pauli, S. A.; Patterson, B. D.; Marchini, S.; Wintterlin, J.; Moritz, W.; Greber, T. *Phys. Rev. Lett.* **2008**, *101*, 126102.
(10) Vázquez de Parga, A. L.; Calleja, F.; Borca, B.; Passeggi, M. C. G.; Hinarejos, J. J.; Guinea, F.; Miranda, R. *Phys. Rev. Lett.* **2008**, *100*, 056807.
(11) Marchini, S.; Günther, S.; Wintterlin, J. *Phys. Rev. B* **2007**, *76*, 075429.
(12) Coraux, J.; Diaye, A. T.; Busse, C.; Michely, T. *Nano Lett.* **2008**, *8*, 565–570.
(13) N'Diaye, A. T.; Bleikamp, S.; Feibelman, P. J.; Michely, T. *Phys. Rev. Lett.* **2006**, *97*, 215501.
(14) Yu, Q.; Lian, J.; Siriponglert, S.; Li, H.; Chen, Y. P.; Pei, S. *Appl. Phys. Lett.* **2008**, *93*, 113103–3.
(15) Reina, A.; Jia, X.; Ho, J.; Nezich, D.; Son, H.; Bulovic, V.; Dresselhaus, M. S.; Kong, J. *Nano Lett.* **2009**, *9*, 30–35.
(16) Kim, K. S.; Zhao, Y.; Jang, H.; Lee, S. Y.; Kim, J. M.; Kim, K. S.; Ahn, J.; Kim, P.; Choi, J.; Hong, B. H. *Nature* **2009**, *457*, 706–710.
(17) Usachov, D.; Dobrotvorskii, A. M.; Varykhalov, A.; Rader, O.; Gudat, W.; Shikin, A. M.; Adamchuk, V. K. *Phys. Rev. B* **2008**, *78*, 085403.
(18) Cao, H.; Yu, Q.; Colby, R.; Pandey, D.; Park, C. S.; Lian, J.; Zemlyanov, D.; Childres, I.; Drachev, V.; Stach, E. A.; Hussain, M.; Li, H.; Pei, S. S.; Chen, Y. P. *J. Appl. Phys.* **2010**, *107*, 044310.

(19) Bae, S.; Kim, H.; Lee, Y.; Xu, X.; Park, J.; Zheng, Y.; Balakrishnan, J.; Lei, T.; Ri Kim, H.; Song, Y. I.; Kim, Y.; Kim, K. S.; Ozyilmaz, B.; Ahn, J.; Hong, B. H.; Iijima, S. *Nat. Nanotechnol.* **2010**, *5*, 574–578.
(20) Emtsev, K. V.; Bostwick, A.; Horn, K.; Jobst, J.; Kellogg, G. L.; Ley, L.; McChesney, J. L.; Ohta, T.; Reshanov, S. A.; Rohrl, J.; Rotenberg, E.; Schmid, A. K.; Waldmann, D.; Weber, H. B.; Seyller, T. *Nat. Mater.* **2009**, *8*, 203–207.
(21) Ni, Z. H.; Chen, W.; Fan, X. F.; Kuo, J. L.; Yu, T.; Wee, A. T. S.; Shen, Z. X. *Phys. Rev. B* **2008**, *77*, 115416.
(22) Geim, A. K. *Science* **2009**, *324*, 1530–1534.
(23) Müller, F.; Sachdev, H.; Hüfner, S.; Pollard, A. J.; Perkins, E. W.; Russell, J. C.; Beton, P. H.; Gsell, S.; Fischer, M.; Schreck, M.; Stritzker, B. *Small* **2009**, *5*, 2291–2296.
(24) Pollard, A. J.; Perkins, E. W.; Smith, N.; Saywell, A.; Goretzki, G.; Phillips, A.; Argent, S.; Sachdev, H.; Müller, F.; Hüfner, S.; Gsell, S.; Fischer, M.; Schreck, M.; Osterwalder, J.; Greber, T.; Berner, S.; Champness, N. R.; Beton, P. H. *Angew. Chem., Int. Ed.* **2010**, *49*, 1794–1799.
(25) Pollard, A. J.; Nair, R. R.; Sabki, S. N.; Staddon, C. R.; Perdigao, L. M. A.; Hsu, C. H.; Garfitt, J. M.; Gangopadhyay, S.; Gleeson, H. F.; Geim, A. K.; Beton, P. H. *J. Phys. Chem. C* **2009**, *113*, 16565–16567.
(26) Zheng, M.; Takei, K.; Hsia, B.; Fang, H.; Zhang, X.; Ferralis, N.; Ko, H.; Chueh, Y.; Zhang, Y.; Maboudian, R.; Javey, A. *Appl. Phys. Lett.* **2010**, *96*, 063110.
(27) Shelton, J.; Patil, H.; Blakely, J. *Surf. Sci.* **1974**, *43*, 493–520.
(28) Eizenberg, M.; Blakely, J. *Surf. Sci.* **1979**, *82*, 228–236.
(29) Fujita, D.; Yoshihara, K. *J. Vac. Sci. Technol. A* **1994**, *12*, 2134.
(30) Fujita, D.; Ohgi, T.; Onishi, K.; Kumakura, T.; Harada, M. *Jpn. J. Appl. Phys.* **2003**, *42*, 1391–1394.
(31) Sun, Z.; Yan, Z.; Yao, J.; Beitler, E.; Zhu, Y.; Tour, J. M. *Nature* **2010**, *468*, 549–552.
(32) Kusch, C.; Winter, B.; Mitzner, R.; Gomes Silva, A.; Campbell, E. E. B.; Hertel, I. V. *Chem. Phys. Lett.* **1997**, *275*, 469–476.
(33) Cepek, C.; Goldoni, A.; Modesti, S. *Phys. Rev. B* **1996**, *53*, 7466.
(34) Blake, P.; Hill, E. W.; Neto, A. H. C.; Novoselov, K. S.; Jiang, D.; Yang, R.; Booth, T. J.; Geim, A. K. *Appl. Phys. Lett.* **2007**, *91*, 063124-3.
(35) Ferrari, A. C.; Meyer, J. C.; Scardaci, V.; Casiraghi, C.; Lazzeri, M.; Mauri, F.; Piscanec, S.; Jiang, D.; Novoselov, K. S.; Roth, S.; Geim, A. K. *Phys. Rev. Lett.* **2006**, *97*, 187401-4.
(36) Kumar, S.; McEvoy, N.; Lutz, T.; Keeley, G. P.; Nicolosi, V.; Murray, C. P.; Blau, W. J.; Duesberg, G. S. *Chem. Commun.* **2010**, *46*, 1422.
(37) Hofrichter, J.; Szafranek, B. N.; Otto, M.; Echtermeyer, T. J.; Baus, M.; Majerus, A.; Geringer, V.; Ramsteiner, M.; Kurz, H. *Nano Lett.* **2010**, *10*, 36–42.